

Stolt's f - k Migration for Plane Wave Ultrasound Imaging

Damien Garcia, Louis Le Tarnec, Stéphan Muth, Emmanuel Montagnon,
Jonathan Porée, and Guy Cloutier

Abstract—Ultrafast ultrasound is an emerging modality that offers new perspectives and opportunities in medical imaging. Plane wave imaging (PWI) allows one to attain very high frame rates by transmission of planar ultrasound wavefronts. As a plane wave reaches a given scatterer, the latter becomes a secondary source emitting upward spherical waves and creating a diffraction hyperbola in the received RF signals. To produce an image of the scatterers, all the hyperbolas must be migrated back to their apexes. To perform beamforming of plane wave echo RFs and return high-quality images at high frame rates, we propose a new migration method carried out in the frequency-wavenumber (f - k) domain.

The f - k migration for PWI has been adapted from the Stolt migration for seismic imaging. This migration technique is based on the exploding reflector model (ERM), which consists in assuming that all the scatterers explode in concert and become acoustic sources. The classical ERM model, however, is not appropriate for PWI. We showed that the ERM can be made suitable for PWI by a spatial transformation of the hyperbolic traces present in the RF data. *In vitro* experiments were performed to outline the advantages of PWI with Stolt's f - k migration over the conventional delay-and-sum (DAS) approach. The Stolt's f - k migration was also compared with the Fourier-based method developed by J.-Y. Lu.

Our findings show that multi-angle compounded f - k migrated images are of quality similar to those obtained with a state-of-the-art dynamic focusing mode. This remained true even with a very small number of steering angles, thus ensuring a highly competitive frame rate. In addition, the new FFT-based f - k migration provides comparable or better contrast-to-noise ratio and lateral resolution than the Lu's and DAS migration schemes. Matlab codes for the Stolt's f - k migration for PWI are provided.

I. INTRODUCTION

CONVENTIONAL medical ultrasound imaging consists in scanning a medium using a series of successive focused or multi-focused beams sweeping along the region of

Manuscript received March 18, 2013; accepted June 17, 2013. This work was supported by a grant from the Canadian Institutes of Health Research (MOP-106465). D. Garcia holds a research scholarship from the Fonds de Recherche en Santé du Québec (FRSQ).

The authors are with the University of Montreal Hospital Research Center (CRCHUM), Montreal, QC, Canada (e-mail: garcia.damien@gmail.com).

D. Garcia, L. Le Tarnec, and S. Muth are also with the Research Unit of Biomechanics and Imaging in Cardiology (RUBIC), University of Montreal Hospital, Montreal, QC, Canada.

D. Garcia and G. Cloutier are also with the Department of Radiology, Radio-Oncology, and Nuclear Medicine, and the Institute of Biomedical Engineering, University of Montreal, Canada.

E. Montagnon, J. Porée, and G. Cloutier are also with the Laboratory of Biorheology and Medical Ultrasonics (LBUM), University of Montreal Hospital, Montreal, QC, Canada.

DOI <http://dx.doi.org/10.1109/TUFFC.2013.2771>

interest. The resulting scanlines are then stacked together to reconstruct a single image. The time required to build one frame is thus proportional to the number of gathered lines and the maximal imaging depth. Technological advances within the last decade (parallel computing, high-performance data transfer, high-speed processors, etc.) now allow production of ultrasound scanners able to generate a full image from a single transmit, thus offering the opportunity for ultrafast imaging. One method to get ultrafast images is by means of plane wave insonifications [1]: a planar wavefront is generated by exciting the transducer elements equally, and the RF echoes are acquired simultaneously by each element to reconstruct an image in post-processing. Whereas focusing approaches concentrate the acoustic energy at one or several locations, plane wave generation tends to minimize the differences in amplitude and phase over the cross-section delimited by the wavefront. Contrarily to conventional ultrasound imaging, the frame rate reached by plane wave ultrasonography is only limited by the time required for a wave to make a two-way trip. Theoretically, frame rates up to 15000 Hz can thus be attained for a 5-cm imaging depth [2]. Recent studies indicate the growing emergence of ultrasound plane wave imaging (PWI). This technique has proven itself as a reliable method in several original and promising applications such as transient elastography, ultrafast Doppler imaging, ultrafast vector flow mapping, electromechanical wave imaging, and functional brain imaging [3]–[7].

As the downward plane wave reaches a single point scatterer, the latter becomes a secondary source emitting upward waves (Fig. 1). Assuming a constant speed of sound within the medium, this source gives rise to a hyperbolic travel-time curve whose eccentricity is governed by the scatterer depth (Fig. 1): the deeper the scatterer, the flatter the hyperbola. More generally, each point scatterer within the insonified medium generates a diffraction hyperbola. The hyperbola thus represents the inhomogeneous point spread function for PWI. To produce an image of the scatterers, these diffraction hyperbolas must be coalesced back into their apexes. In this manuscript, by analogy with seismic imaging, this beamforming process is called *migration*.

Migration improves focusing by essentially achieving amplitude and phase rectifications to correct for the effects of the spreading of ray paths as waves propagate [8]. In its simplest form, migration by summation of trace amplitudes along hyperbolic trajectories (known as diffraction summation) has been a basic tool for geophysicists since the 1950s [9]. This method has been extensively used

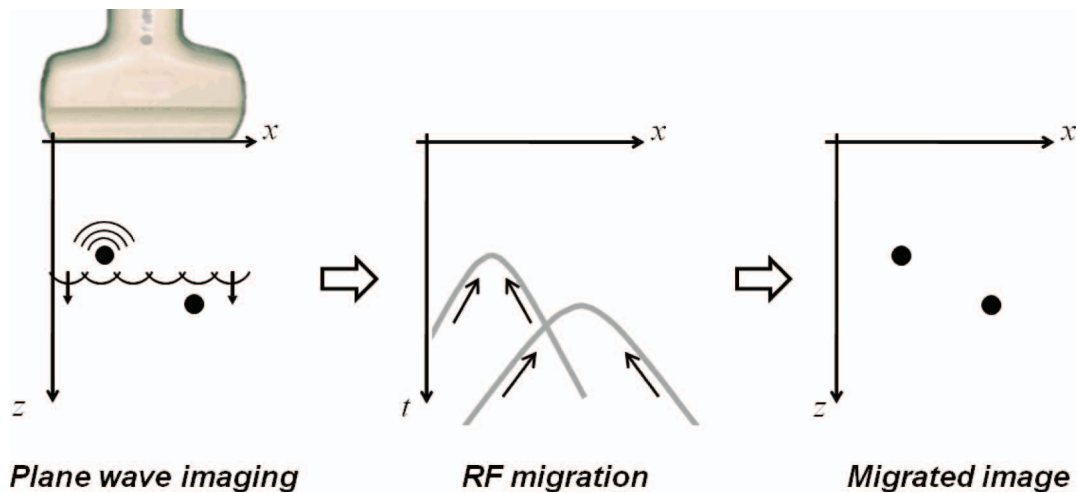


Fig. 1. Migration process for plane wave imaging. As the scatterers are reached by a plane wave, they become secondary sources that emit upward spherical waves and generate diffraction hyperbolas in the RF backscattered signals. Migration allows one to recover the scatterers' positions and to reconstruct a B-mode image. 

in ultrasound imaging under the name delay-and-sum (DAS). Adapting this approach to the context of PWI, Montaldo *et al.* thoroughly described a migration technique based on the two-way travel times for an acoustic wave to reach a scatterer and get back to the transducer elements [1]. The DAS simply consists in integrating the ultrasound RF signals over all the hyperbolas present in the RF signals. The pixels of the resulting migrated RF image are thus assigned the integral values. To potentially improve the image quality and increase the computational efficiency of PWI migration, we propose a new migration method carried out in the frequency-wavenumber (f - k) domain, thus bringing the benefit of much faster computational speed, resulting from the use of the fast Fourier transform (FFT) algorithm, while keeping high contrast-to-noise ratio (CNR) and lateral resolution. The f - k migration for PWI is inspired by the original Fourier migration introduced by Stolt for seismic imaging [10], [11]. Section II demonstrates how the standard Stolt's method is adapted for plane wave insonifications.

FFT-based beamforming for ultrasonic imaging has been the topic of numerous studies since the early 1980s [12]–[19]. Most of them are based on the angular spectrum method, which consists in decomposing the reflected wavefield into plane waves, each propagating at a different angle. Although originally derived for monochromatic waves, the angular spectrum method has been extended to wideband systems [13], [14]. Much more computationally efficient FFT-based approaches have been recently inspired from the synthetic aperture radar/sonar (SAR/SAS) community [20]–[22]. These techniques, sometimes referred to as wavenumber algorithms, solve the focusing problem using one-dimensional interpolations in the Fourier domain [12], [17]–[19]. Although extensively applied for imaging in SAR/SAS, the wavenumber algorithm was originally developed by Stolt for exploration seismology [10]. None of the aforementioned studies, however, fall within the scope of PWI. Instead, each single element

of the transducers must be fired independently, while one or several elements are used in reception, thus somewhat mimicking the ideal zero-offset seismic configuration [10], [12]. To reach very high frame rates, an FFT-based reconstruction of ultrasound images obtained by plane wave insonifications has been successfully addressed by J.-Y. Lu and his team [23]–[25]. This spectral technique has recently been tested by an independent group [26]. In Lu's method, the RF image is essentially remapped in the Fourier domain by interpolating the temporal frequencies. This approach is based on the assumption that the scatterers all behave as monopole sources [27].

In this manuscript, we derive a new Fourier f - k migration technique for plane wave ultrasound imaging by modifying the so-called exploding reflector model. *In vitro* results are presented to outline the benefits of the Stolt's f - k migration, in terms of image quality, over dynamic focusing and DAS. The new f - k migration process is also compared with Lu's method. The differences between the three approaches (DAS, f - k migration, and Lu's method) are discussed in Section IV. A concise and readable Matlab code (The MathWorks Inc., Natick, MA) for the f - k migration is given in the Appendix for the readers familiar with Matlab to grasp the underlying algorithm. In addition, a complete optimized Matlab code with *in vitro* examples is provided in the online supplementary content () and in [28].

II. THEORETICAL BACKGROUND: ADAPTING THE FOURIER DOMAIN STOLT'S MIGRATION FOR PLANE WAVE IMAGING

A. The Exploding Reflector Model for Plane Wave Imaging

The classical seismic Stolt's f - k migration is based on the exploding reflector model (ERM), which assumes that

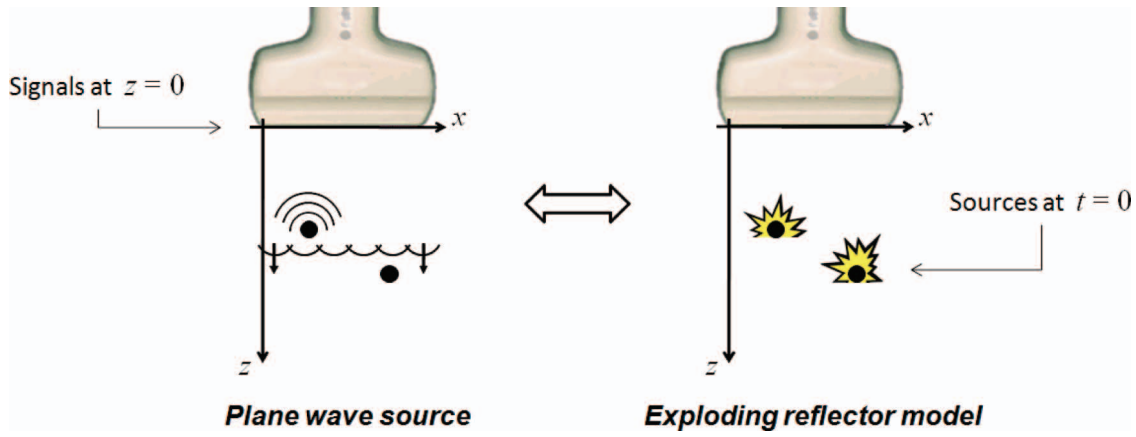


Fig. 2. The exploding reflector model (ERM). In the ERM, the scatterers are assumed to explode in concert, which simplifies the time-reversal problem. To obtain the scatterers' positions, one must determine the wavefield at the time of explosion. In this study, the ERM, originally introduced for the seismic zero-offset configuration, is adapted to plane wave imaging.

all the reflectors in the medium explode simultaneously and become upward-emitting acoustic sources (Fig. 2) [29]. This postulate reduces the back-and-forth wave propagation to an upward wave scenario. The f - k migration then attempts to time-reverse the wave propagation and determine the ERM wavefield at $t = 0$ (i.e., at the time of explosion) based on the sole knowledge of the wavefield on the surface $z = 0$ (Fig. 2). In order for the acoustic wavefield to be properly migrated, the ERM must reflect the actual two-way propagation accurately; in other words, one must seek the exploding sources whose ERM-based hyperbolas fit the actual RF hyperbolas. The f - k migration precisely consists in applying the Stolt method to find these virtual sources, followed by a spatial transformation to recover the actual scatterers' positions. This process is straightforward in the particular zero-offset configuration because one simply must halve the wavefield propagation speed (see the following subsection). In the context of PWI, however, the classical ERM is not suitable as it stands, but the exploding model turns out to be well adaptable to plane wave insonification, as explained in the next subsections. Let us first mention that there is no delay in reception in the following.

1) *The Simplest Case: The One Emitter-Receiver Element Scenario:* This situation is equivalent to the so-called zero-offset section encountered in post-stack migration for seismic imaging [30]. Such a zero-offset section is acquired by moving a single coincident emitter/receiver along the recording surface. For ultrasound imaging, by analogy, each element of the transducer both transmits the impulse signals and receives the RF echoes, one at a time. As a recent example, this seismic imaging concept was applied for nondestructive industrial evaluation of multi-layered media [19]. In this specific configuration, a scatterer positioned at (x_s, z_s) leads to a two-way travel-time (from emitter to scatterer back to receiver) which depends upon the transducer position x and is characterized by the hyperbola given by

$$\tau_s(x) = \frac{2}{c} \sqrt{(x_s - x)^2 + z_s^2}. \quad (1)$$

We use here the notation (x_s, z_s) relative to a linear array: x_s stands for the scatterer position parallel to the array and z_s represents its depth position relative to the array. The origin $(0, 0)$ is located at the center of the first left-most element. The wave propagation speed (c) is assumed constant in the insonified tissues. The factor 2 in (1) reflects the round-trip of the wavefield through the medium. It is now easy to see that an exploding source at (\hat{x}_s, \hat{z}_s) within a medium whose propagation speed is \hat{c} (this is a one-way situation, from scatterer to receiver) yields the following ERM travel-time:

$$\hat{\tau}_s(x) = \frac{1}{\hat{c}} \sqrt{(\hat{x}_s - x)^2 + \hat{z}_s^2}. \quad (2)$$

Making equal the travel-times τ_s (1) and $\hat{\tau}_s$ (2) by choosing $(\hat{x}_s, \hat{z}_s) = (x_s, z_s)$ and halving the propagation speed (i.e., $\hat{c} = c/2$) makes the ERM and the one emitter-receiver scenario alike.

2) *The ERM With a Horizontal Plane Wave:* To generate a horizontal plane wave, all the transducer elements must emit synchronously. We thus leave the simple aforementioned scenario. Assuming that a horizontal plane wave is sent within the medium, the travel-time produced by a scatterer positioned at (x_s, z_s) is now given by (see [1] for details):

$$\hat{\tau}_s(x) = \frac{1}{c} (z_s + \sqrt{(x_s - x)^2 + z_s^2}). \quad (3)$$

To make the ERM compatible with the horizontal plane wave acquisition, one must fit the hyperbolas given by (2) and (3). No simple relation, however, can provide a perfect fitting. Because most of the signal energy is concentrated around the apex of the hyperbola, a compromise is to make equal their apical zeroth- to second-order deriva-

tives. This is done by equalizing τ_s and $\hat{\tau}_s$ as well as their first and second derivatives (with respect to x) at $x = x_s$ ($= \hat{x}_s$), respectively, which yields

$$\hat{c} = \frac{\sqrt{2}}{2}c, \quad \text{and} \quad \hat{z}_s = \sqrt{2}z_s. \quad (4)$$

In the particular case of a horizontal plane wave, the expressions in (4) make the ERM compatible with PWI. In comparison with the one emitter-receiver element scenario, the wavefield propagation speed must not be simply halved; in addition, the depth must be rescaled. These relations make the travel times given by (2) and (3) almost equal in the vicinity of the apex, and their difference decreases in $O((x - x_s)^4)$. The phase error— $\Delta\varphi_s = 2\pi f_0|\tau_s(x) - \hat{\tau}_s(x)|$, where f_0 is the central frequency—related to this approximation in the travel times is illustrated in Fig. 3. One can observe that the phase errors are larger for large obliquities (i.e., for large deviation angles formed by the scatterer with respect to the transducer element). This, however, is expected to have little effects on the migrated images because the reflected acoustic energy is maximal for small obliquity values.

3) *The General Case: The ERM With a Tilted Plane Wave:* In practice, because the image quality achieved with a single plane wave is suboptimal [1], several slightly tilted consecutive plane wavefronts are transmitted and the backscattered RF signals are coherently compounded. It has been reported that less than 10 angles can provide PWI-derived images with quality similar to standard multi-focus methods, thus ensuring a highly competitive frame rate [1]. To be able to perform multi-angle compounding with our method, it must be ensured that the ERM can be adapted to a slant plane wave as well. For a

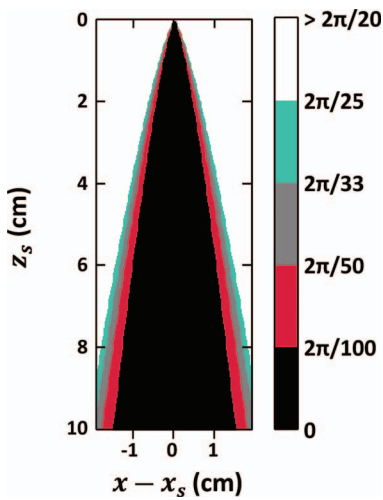


Fig. 3. Phase errors induced to exploding reflector model (ERM) modification. The travel-times of the classical ERM have been modified to make the ERM model adapted to plane wave imaging. The phase errors induced by these approximations depend upon the scatterer depth (z_s) and on its position relative to the transducer element ($x - x_s$). A 5 MHz central frequency was used.

plane wave tilted with an angle θ from the horizontal [see Fig. 4(a)], the travel time becomes (see [1] for details):

$$\tau_s(x) = \frac{1}{c}(\sin(\theta)x_s + \cos(\theta)z_s + \sqrt{(x_s - x)^2 + z_s^2}). \quad (5)$$

As performed in the previous paragraph, one now wants to fit this hyperbola with the ERM-based hyperbola given by (2). Again, a perfect fitting cannot be obtained and the strategy is to seek simple transformations that establish the equality of the zeroth- to second-order derivatives. To do so, the RF echoes are first trimmed to eliminate the leading zero signals caused by the emission delays (see Fig. 4). The travel time (5) thus becomes:

$$\tau_s(x) = \frac{1}{c}(\sin(\theta)(x_s - x) + \cos(\theta)z_s + \sqrt{(x_s - x)^2 + z_s^2}). \quad (6)$$

Now, let (α, β, γ) be constant parameters defined by

$$\begin{cases} \hat{c} = \alpha c \\ \hat{z}_s = \beta z_s \\ \hat{x}_s = x_s + \gamma z_s. \end{cases} \quad (7)$$

Using the definitions in (7), the ERM travel time given by (2) becomes:

$$\hat{\tau}_s(x) = \frac{1}{\alpha c} \sqrt{(x_s + \gamma z_s - x)^2 + \beta^2 z_s^2}. \quad (8)$$

Equalizing τ_s (6) and $\hat{\tau}_s$ (8), as well as their first and second derivatives at $x = x_s$, provides the following expressions:

$$\begin{cases} \alpha = 1/\sqrt{1 + \cos(\theta) + \sin^2(\theta)} \\ \beta = \frac{(1 + \cos(\theta))^{3/2}}{1 + \cos(\theta) + \sin^2(\theta)} \\ \gamma = \frac{\sin(\theta)}{2 - \cos(\theta)}. \end{cases} \quad (9)$$

Note that we get $(\alpha, \beta, \gamma) = (\sqrt{2}/2, \sqrt{2}, 0)$ when $\theta = 0$, as obtained with the horizontal wavefront (4). The ERM in conjunction with the transformations defined by (7) and (9) can thus be used to model tilted PWI. The difference between the travel times given by (6) and (8) decreases in $O((x - x_s)^3)$.

We have just seen that the ERM can be generalized to model PWI adequately. This is a major point because the ERM is the key element of the f - k migration described next. The whole process is diagrammed in Fig. 4.

B. Stolt's f - k Migration

The goal of the migration process is to reconstruct ultrasound images from the raw RF signals generated in PWI mode. Montaldo *et al.* recently introduced and successfully tested a DAS method defined in the time-space

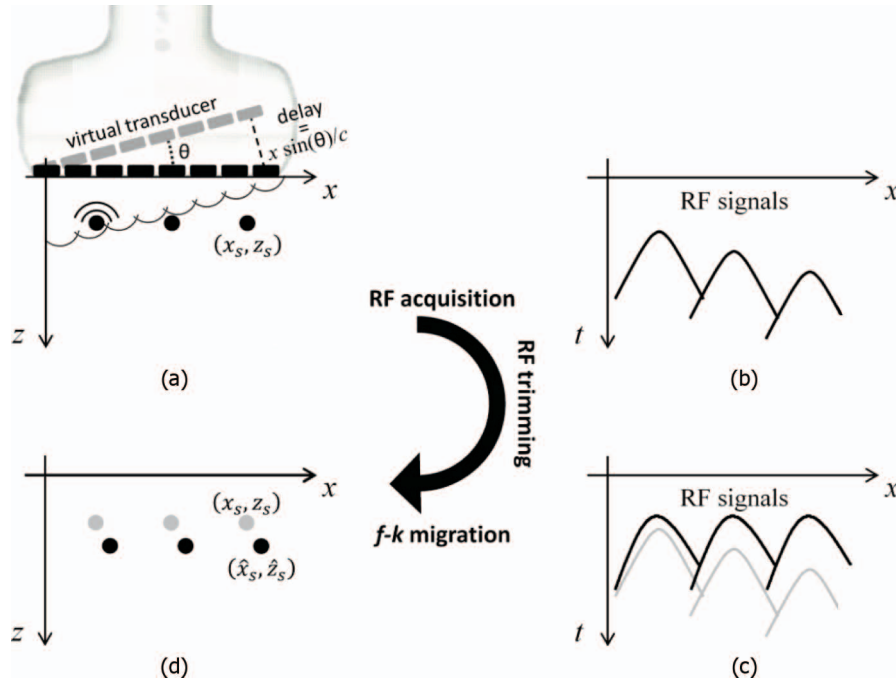


Fig. 4. Adapting the f - k migration to tilted plane wave imaging. (a) A slant plane wave is emitted. In this example, the leftmost scatterer is the first to perceive the planar wavefield. (b) The resulting diffraction hyperbolas in the RF echoes are not aligned. (c) Trimming the RF signals realigns the hyperbolas horizontally (from gray to black). (d) A scatterer originally located at (x_s, z_s) will be moved to (\hat{x}_s, \hat{z}_s) after the f - k migration. 

domain [1]. Lu *et al.* proposed a Fourier-based approach [25]. We now propose a new migration method that also operates entirely in the Fourier frequency-wavenumber domain (f - k migration).

In the field of seismic imaging, Stolt proposed in 1978 a migration method, commonly called the f - k (or sometimes ω - k) migration, allowing the construction of migrated images in the frequency domain [10]. The Stolt f - k migration is currently, by a wide margin, the fastest migration technique but it is limited to a constant propagation wave velocity [11]. Although it can be a major drawback in seismology, in which propagation speeds may vary by a factor of 5 (typically from 1000 to 5000 m/s [31]), this constraint is generally less critical in most situations for medical ultrasound, in which the speed of sound remains around 1500 m/s in soft tissues (typically from 1480 to 1670 m/s [32]). The f - k migration was developed from the linear wave equation using Fourier transforms. We invite readers to refer to [8] for a well-written and complete description of the Stolt f - k migration. Only the main steps are described here.

Let $\Psi(x, z, t)$ be a scalar wavefield of the ERM satisfying the linear two-dimensional wave equation. One wants to determine the ERM wavefield at the time of explosion, i.e., $\Psi(x, z, t = 0)$, knowing the wavefield on the surface $\Psi(x, z = 0, t)$. Let $\phi(k_x, z, f)$ denote the Fourier transform of $\Psi(x, z, t)$ over (x, t) , so that

$$\Psi(x, z, t) = \iint_{-\infty}^{+\infty} \phi(k_x, z, f) e^{2i\pi(k_x x - ft)} dk_x df, \quad (10)$$

where k_x stands for the spatial wavenumber related to x and f is the temporal frequency. For a constant ERM propagation speed (\hat{c}), the application of the Fourier transform to the wave equation yields the following Helmholtz equation [8]:

$$\frac{\partial^2 \phi}{\partial z^2} + 4\pi^2 \hat{k}_z^2 \phi = 0, \quad (11)$$

where the wavenumber \hat{k}_z is given by

$$\hat{k}_z^2 = \frac{f^2}{\hat{c}^2} - k_x^2. \quad (12)$$

The unique boundary condition for (11) is $\phi(k_x, 0, f)$, which is the Fourier transform of $\Psi(x, z = 0, t)$. To close the ERM migration problem described by (11) and (12), it is now assumed that $\Psi(x, z, t)$ contains only waves moving upward (see [8, Eq. 5.48]). The ERM wavefield is thus allowed to propagate on the $-z$ direction only, as would occur with primary reflections. The wave equation can thus be solved and one obtains the migrated wavefield [8]:

$$\Psi(x, z, 0) = \iint_{-\infty}^{+\infty} \phi(k_x, 0, f) e^{2i\pi(k_x x - \hat{k}_z z)} dk_x df. \quad (13)$$

To fully benefit from the Fourier transforms, Stolt proposed to change the variable \hat{k}_z by introducing [see (12)]

$$f(\hat{k}_z) = \hat{c} \text{sign}(\hat{k}_z) \sqrt{k_x^2 + \hat{k}_z^2}. \quad (14)$$

This expression describes the spectral remapping of the Stolt's f - k migration for PWI, which differs from the re-mapping proposed by Lu [25] (more details are given in Section IV-A). Using the change of variables (14), the Stolt's migration solution is finally

$$\Psi(x, z, 0) = \iint_{-\infty}^{+\infty} \frac{\hat{k}_z}{\sqrt{k_x^2 + \hat{k}_z^2}} \phi(k_x, 0, f(\hat{k}_z)) e^{2i\pi(k_x x - \hat{k}_z z)} dk_x d\hat{k}_z. \quad (15)$$

As shown by (15), the migrated solution is basically the inverse Fourier transform of

$$\frac{\hat{k}_z}{\sqrt{k_x^2 + \hat{k}_z^2}} \phi(k_x, 0, f(\hat{k}_z)). \quad (16)$$

C. The Stolt's f - k Migration Algorithm for Plane-Wave Ultrasound Imaging

We have just seen how to adapt the exploding reflector model (ERM) for plane-wave ultrasound imaging (PWI) in Section II-A. We also showed that the migrated solution of the ERM is given by (15). We now have the framework for the f - k migration of PWI-derived RF signals. The three-step process to get f - k migrated images can be summarized as follows:

- 1) The leading zeros of the RF signals resulting from the emission delays are first removed (6). This is step (b) to (c) in Fig. 4. This signal trimming aligns the hyperbolas of same apical curvature horizontally [Fig. 4(c)]. Note that this operation slightly distorts the hyperbolas [Fig. 4(c)], distorting them more for larger steering angles.
- 2) The Stolt's migration algorithm described by (14) and (15) is applied [steps (c) to (d) in Fig. 4] using the ERM velocity \hat{c} as defined in (7) and (9). A scatterer originally located at (x_s, z_s) will be moved to (\hat{x}_s, \hat{z}_s) after the migration [Fig. 4(d)]
- 3) Coordinate transformations $(\hat{x}_s, \hat{z}_s) \rightarrow (x_s, z_s)$ are performed to get back into the actual position [Fig. 4(d)] by using the expressions given by (7) and (9).

It is worth noting that these basic steps can be implemented in the Fourier domain to gain significant computational speed. A pseudo-code for tilted PWI f - k migration is proposed in Fig. 5 and a simplified Matlab code (for horizontal plane waves only) is given in the Appendix. A complete and optimized Matlab pcode (protected function file) is also provided in the supplementary materials (Fig. 6) and in [28]. This latter program was used to generate the f - k migrated images contained in this manuscript.

As illustrated by (12) and (15), the Stolt's migration includes a nonuniform Fourier transform because the \hat{k}_z s are not equally sampled. To gain computational speed by

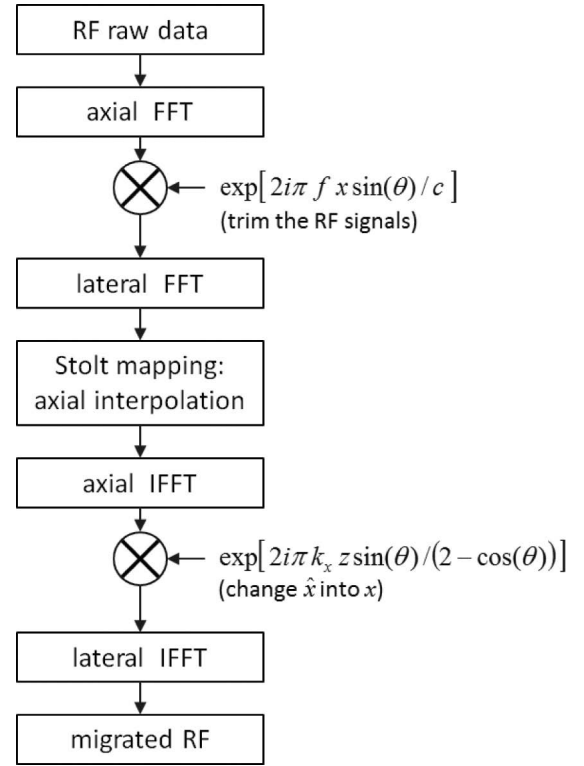


Fig. 5. Diagram of the Stolt's f - k migration algorithm for plane wave imaging. The proposed algorithm for migration of the RF signals works entirely in the Fourier domain. The coordinates x and z are defined as in Fig. 4. The parameters k_x and f stand for the spatial wavenumber and the temporal frequency, respectively. The wavefront angle θ is defined relative to the transducer (see Fig. 4).

using the fast Fourier transform (FFT), the data must be laid on a regular grid by interpolation or other gridding methods, as performed in geosciences or magnetic resonance imaging [33]–[36]. In our context, the simplest algorithm consisted of linear interpolation after extensive zero-padding in the first FFT: $\Psi(x, z = 0, t) \rightarrow \phi(k_x, 0, f)$. Although a nonuniform FFT [26], [35] could have been included in the f - k migration algorithm, we instead used a linear interpolation scheme for the sake of simplicity. As an alternative, the sinc (sine cardinal) interpolation could also be used to reduce the amount of zero-padding and make the algorithm a bit faster [34]. The sinc interpolator option is available in the Matlab pcode given in the Supplementary materials (Fig. 6).

III. IN VITRO EXPERIMENTS: STOLT'S F - K MIGRATION AGAINST DAS AND LU'S METHOD

As detailed in this section, ultrasound PWI was analyzed in an *in vitro* phantom to illustrate the performance of the new f - k algorithm for migrating PWI-derived RF data. *In vitro* plane wave measurements were performed with the Verasonics research scanner (V-1-128, Verasonics Inc., Redmond, WA). The raw RF signals were trans-

formed using the DAS [1], the f - k migration and the Lu's method [25]. The reconstructed B-mode images were compared with those obtained using state-of-the-art dynamic multi-focusing approaches. The f - k migration and the Lu's method were compared under strictly similar conditions. Only the spectral remapping formulas (see Section IV-A for more details) were different in the algorithms. Other conditions that may affect image quality (interpolation schemes, FFT, zero-padding, etc.) were kept unchanged.

A. Construction of the Migrated Images

In vitro RF data were acquired with the V-1 Verasonics scanner using a 5-MHz linear-array transducer (ATL L7-4, 128 elements, pitch = 0.3 mm) and the 403GS LE Gammex phantom (Gammex Inc., Middleton, WI). The Gammex phantom was insonified with successive tilted plane waves. No transmit apodization was used. RF raw data backscattered by anechoic mimicking cysts and 0.1-mm nylon fibers up to 10 cm deep were acquired at a sampling frequency of 20 MHz. The RF signals were zero-phase high-pass filtered to remove any dc offset. The RFs were then migrated using the DAS, f - k , and Lu's methods. An f -number of 1.75 (i.e., the maximal aperture was given by $z/f = z/1.75$) was used when beamforming with the DAS to make the contrast better in the very near field [1]. The migrated RF signals were time-gain compensated and B-mode images were obtained through a Hilbert transform. The B-mode images were gamma-compressed using $\gamma = 0.3$ (except for the study of lateral resolution, see Section III-D) and converted to 8-bit grayscale. To assess the quality of the images generated by ultrasound plane waves, PWI was compared with the dynamic focusing mode offered by the Verasonics scanner. In the latter approach, 128 dynamically focused scanlines were obtained using seven transmit foci vertically distributed over the region-of-interest, and an f -number of 1.75 (as in [1]).

B. Effect of the Steering Angle on the CNR

Multi-angle RF coherent compounding is required with plane wave imaging (PWI) to enhance the quality of the ultrasound images [1]. We first verified the quality of PWI-derived B-mode images returned by a single plane wave insonification with a given wavefront angle (defined with respect to the transducer). The manner in which the wavefront angle [denoted θ in (5); see also Fig. 4(a)] affects the CNR of migrated images has been investigated *in vitro* on a single 6-mm-diameter, 3-cm-deep anechoic target. The target CNR in decibels was defined as [37]

$$\text{CNR} = 20 \log_{10} \frac{|\mu_t - \mu_b|}{\sqrt{(\sigma_t^2 + \sigma_b^2)/2}}, \quad (17)$$

where μ_t and μ_b (σ_t^2 and σ_b^2) are the means (variances) of gray levels in the target and the surrounding background, respectively.

The *in vitro* results show that the CNR decreased when the wavefront angle increased (Fig. 6). The CNR remained almost unchanged for wavefront angles varying from 0° to 10° (Fig. 6). Beyond 10° , however, a rapid decrease in CNR was observed with the three migration techniques, which indicates that high wavefront angles (with respect to the probe) should be avoided to obtain high-quality images. In this configuration, no major difference between the three migration methods was noticed below 10° . According to our findings, the absolute wavefront angle for PWI should preferably remain lower than 10° . This observation, however, cannot be generalized because the maximal acceptable steering angle very likely depends upon several factors, such as the central frequency and the pitch. As a side note, the contrast, as defined by [37, Eq. (1)], had a behavior very similar to the contrast-to-noise ratio; see Fig. 6-bis in the online supplementary materials for detailed results (Fig. 6-bis).

C. Effect of the Number of Compounding Angles on the CNR

The combination of several migrated RF signals acquired with different wavefront angles may significantly improve the quality of the resulting image, more importantly for large depths. Getting one image by coherent compounding was carried out as follows: 1) several RF signals were acquired with slightly different plane wave angles; 2) they were migrated independently, then averaged; and 3) an envelope detection was performed in the resulting compounded migrated RF data. To analyze how the number of compounding angles improves the image quality, a series of *in vitro* tests were performed with anechoic mimicking cysts. The angular range was chosen as $[-\theta_{\max}; +\theta_{\max}]$ with an increment of 1° , and θ_{\max} was varied from 0° to 10° . For instance, when θ_{\max} was 3° , seven angles (i.e., $-3^\circ, -2^\circ, -1^\circ, 0^\circ, 1^\circ, 2^\circ, 3^\circ$) were used to create a compounded image. The data acquired by PWI were compared with those obtained by the dynamic focusing mode offered by the Verasonics scanner. The CNR of the targets (3- and 8-cm-deep anechoic cysts), delimited by dashed circles in Fig. 7, was calculated using (17).

As expected, the CNR of the anechoic cysts improved when increasing the number of angles (Fig. 7). This improvement, however, became nonsignificant above a total number of 9 or 11 angles. The *in vitro* results show that the three migration methods perform roughly equally, although the CNR reached by Lu's method was somewhat lower. Our findings also indicate that compounding PWI with f - k migration using a very few angles (typically 7 to 11) equals the dynamic focusing approach in terms of CNR (10.7 and 9.6 dB at 3- and 8-cm-depth, respectively), which ensures a highly competitive frame rate for PWI (only 7 to 11 compounded firing sequences are required) in comparison with the focused imaging ($128 \times$ number-of-foci firing sequences). Similar conclusions were reached with the contrast defined by [37, Eq. (1)]; see Fig.

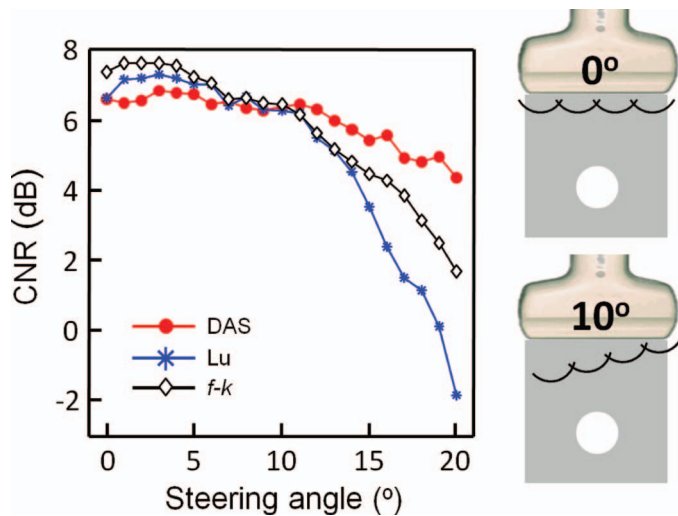


Fig. 6. Effect of the steering angle on the contrast-to-noise ratio. *In vitro* results. Contrast-to-noise ratio (CNR) for a 6-mm-diameter, 3-cm-deep anechoic target (using a Gammex phantom and the Verasonics scanner). The CNR remained unchanged up to 10°, then decreased rapidly with angles >10°, regardless of the migration method [delay-and-sum (DAS), Lu's method, or f - k migration]. See also Fig. 6-bis in the supplementary materials.

7-bis in the online supplementary materials for detailed results ().

D. Analysis of the Lateral Resolution

The effect of the number of compounding angles (from 1 to 21 angles, with an increment of 1°, as in the previous subsection) on the lateral resolution given by PWI was first analyzed at 3 and 8 cm depth. Coherent compounding was performed as described in the previous subsection. The lateral resolution slightly improved with the

DAS and Lu's approaches when increasing the number of compounding angles, both at 3 and 8 cm depth (see Fig. 8). The resolution provided by the two Fourier methods (f - k and Lu's) was better at 8 cm. At 3 cm, the resolution reached with the f - k migration was better with a small number of angles (0.55 mm versus 0.71 mm) and became identical with 21 angles (\approx 0.60 mm).

The lateral resolution provided by PWI was then compared with that given by the dynamic focusing method with the Verasonics scanner and the 128-element linear-array transducer. The effect of the depth on the resolution was assessed *in vitro* using the 0.1-mm nylon fibers (up to 10 cm deep) of the Gammex phantom. Dynamic focusing was obtained using 7 foci and an f -number of 1.75. The lateral resolution was estimated by measuring the full-width at half-maximum (FWHM) of the real envelopes of the migrated RF signals (no gamma-compression was used here).

Seven angles (-3° to 3° , increment of 1°) were used for the compounded PWI images. The PWI-derived lateral resolution was around 0.6 mm (\approx 2 pitches) until about 4 cm deep, then degraded linearly up to 1.25 mm (\approx 4 pitches) at 10 cm (see Fig. 9). The lateral resolution was slightly better with the f - k migration in comparison with the DAS and Lu's method. On average, the lateral resolution achieved by the dynamic focusing mode was better than the f - k migrated PWI (difference = 0.17 ± 0.08 mm = 0.59 ± 0.27 pitch). It is worth noticing, however, that the number of firing sequences was 128 times higher with the dynamic focusing mode. The resolution obtained by PWI in our study (between 0.5 and 1.2 mm) was somewhat similar to that reported by Montaldo *et al.* in [1] (around 1.1 mm at 4.5 MHz with a 0.33 mm pitch). Counterintuitively, however, they did not observe any degradation of the lateral resolution at larger depths. As depth increases, though, the hyperbolas generated by PWI flat-

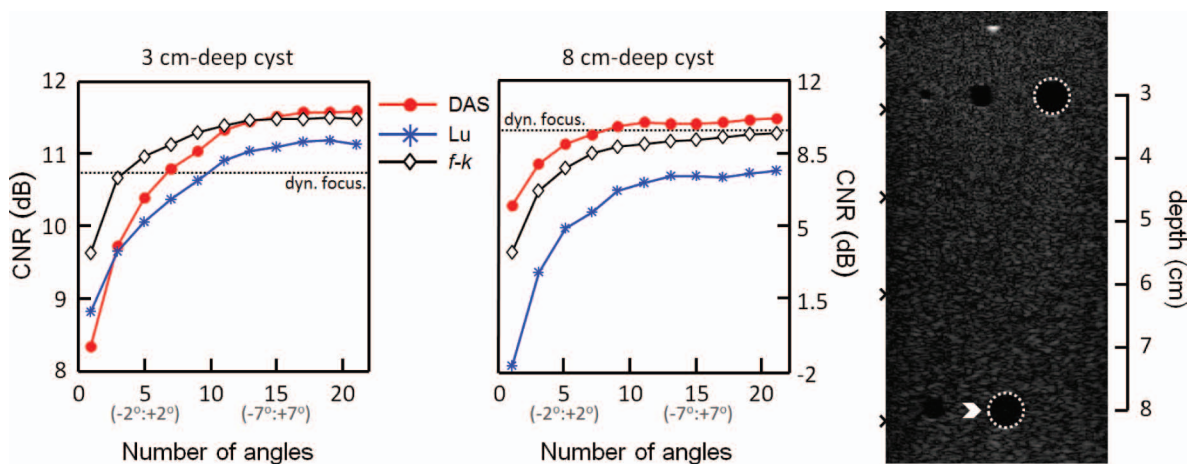


Fig. 7. Effect of the number of compounding angles on the contrast-to-noise ratio. *In vitro* results. Contrast-to-noise ratio (CNR) for 6-mm-diameter, 3- and 8-cm-deep anechoic targets (using a Gammex phantom and the Verasonics scanner). The targets of interest are delimited by dashed circles. Multi-angle compounding plane wave imaging provided CNR similar to those given by the dynamic focusing approach (dyn. focus. in the figure, dashed horizontal lines). The locations of the foci are represented by the left markers in the rightmost image. The rightmost figure was obtained using f - k migration and seven compounding angles. See also Fig. 7-bis in the supplementary materials.

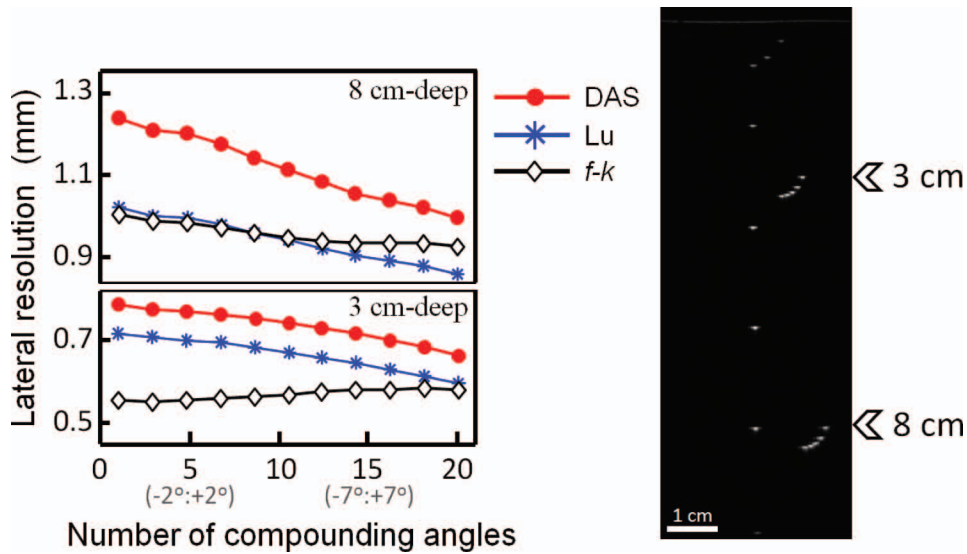


Fig. 8. Effect of the number of compounding angles on the lateral resolution. Lateral resolution at 3 and 8 cm depth reached by multi-angle compounding plane wave imaging (using a Gammex phantom and the Verasonics scanner). The lateral resolution improved with increasing number of compounding angles. See also Fig. 9.

ten (and become a horizontal line at infinite depth), thus producing some ambiguity in the location of their apexes and consequently reducing the lateral resolution.

E. Computational Complexity: Stolt's f - k Migration Versus DAS

To determine the computational complexity of the f - k migration, let n_t denote the number of elements in the transducer (in general, 64, 128, or 192) and n_s denote the number of time samples (typically ≥ 1000 to 3000). The f - k migration requires two 2-D FFTs and the computation of (n_t, n_s) interpolated values. In comparison, the DAS proposed by Montaldo *et al.* must retrieve $n_t(n_t n_s)$ interpolated data and perform $(n_t n_s)$ summations over n_t values [1]. The computational complexity of the migrating process thus decreases from $O(n_t n_t n_s)$ down to $O(n_t n_s \log(n_t n_s))$ when performed in the Fourier domain. Note that Lu's method has the same computational complexity as the f - k migration because only the interpolation scheme is different (see Section IV-A). The number of floating operations is significantly reduced when the migration of the RF data are carried out in the Fourier domain.

Overall, in our study, the f - k migration ran around 25 times faster than the DAS on a CPU (Intel Core i5, Intel Corp., Santa Clara, CA) operating at 2.80 GHz, regardless of the number of time samples. However, it is obvious that the actual resources utilized by the algorithms depend upon numerous aspects, including the programming language, CPU or GPU speed, available memory, speed of data transfer, serial or parallel transfer, etc. Recent works show that GPU platforms can execute beamforming for plane wave imaging at frame rates well beyond the video display range [38]. In this study, because it was not our goal to get real-time visualization, the RF signals were migrated offline using Matlab.

IV. DISCUSSION

Ultrafast ultrasound PWI, in comparison with the conventional focusing approaches, allows one to obtain a full image with a single transmit by migration of the resulting RF signals. We have shown that PWI-derived ultrasound images can offer an image quality similar to that provided by a state-of-the-art dynamic focusing approach, but with a frame rate up to 100 times faster. In the present paper, a well-established seismic migration method—the Stolt's f - k migration—has been modified for PWI. Because we are not in the specific zero-offset condition of seismic imaging, we needed to adapt the exploding reflector model (ERM). We demonstrated that the ERM can be made suitable to PWI by fine-tuning the diffraction hyperbolas present in the RF data. The resulting new f - k migration yielded high-quality images in terms of CNR and lateral resolution.

The main advantage of the f - k migration over conventional DAS is that it works completely in the Fourier space. This makes the algorithm much faster, and any filtering process in the frequency domain can be included without significant increase in computation time. Potential improvements could be further provided to the f - k migration algorithm. As already mentioned, a nonuniform FFT (NUFFT) can be used to get rid of the interpolation process that appears in the Stolt's migration (Fig. 5). As another alternative, because the band-pass RF signals are highly sparse, the f - k migration could be made even faster with the use of sparse Fourier transforms [39], [40]. Although the theory has been derived in two dimensions, the f - k migration for PWI can be generalized in three dimensions. It may be expected that three-dimensional PWI with a 32×32 or 64×64 matrix array would be feasible in the near future. In that case, one would simply have to deal with hyperboloids instead of hyperbolas.

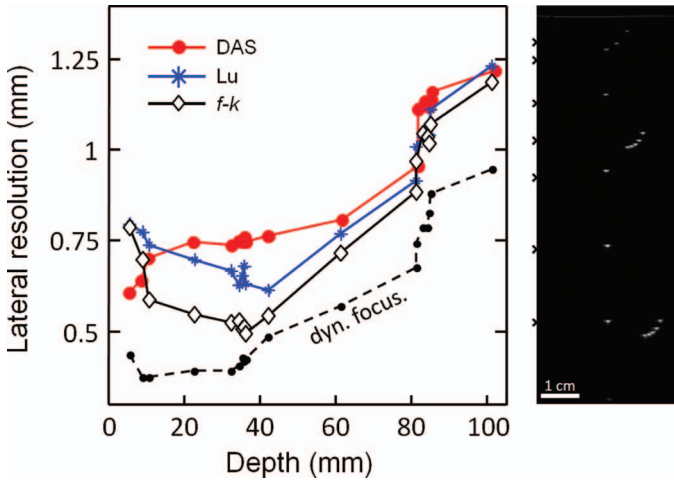


Fig. 9. Effect of depth on the lateral resolution. Seven-angle compounded plane wave images, reconstructed with the different migration methods [Lu's method, delay-and-sum (DAS), or f - k migration], were compared with dynamically focused images in a Gammex phantom using the Verasonics scanner. Only seven firing sequences were used to obtain a plane wave image (see left grayscale image obtained with f - k migration), whereas 896 sequences were needed in the dynamic focusing mode (dyn. focus. in the figure). The locations of the foci used in dynamic focusing are represented by the left markers in the rightmost image.

A. Differences Among the Three Migration Methods

In this study, we have shown that the new FFT-based f - k migration provided comparable or better contrast-to-noise ratio and lateral resolution than the Lu's and DAS migration schemes. One must be aware that migration is an ill-posed inverse problem. The wave equation indeed requires two boundary/initial conditions to be solved. Available information (acoustic pressure at $z = 0$, only) is insufficient to recover the insonified medium. Additional assumptions are thus required to close the problem. The different migration algorithms precisely differ by the kind of approximations made.

1) *DAS*: The DAS is actually equivalent to the so-called diffraction summation, the simplest migration method used by the geophysicists since the 1960s [9]. This is a geometric strategy which consists of summing the backscattered signals along the hyperbolic traces of the diffraction responses. The DAS thus provides a basic solution of the migration problem. Although this procedure makes good sense and provides good outputs in plane wave imaging, it is theoretically incorrect [29]. A more exact process would be, for instance, given by the Kirchhoff's integral theorem, which adds amplitude and phase corrections to the data before summation [29], [41], [42].

2) *Spectral Mapping of the Fourier-Based Methods*: Both Lu and f - k migrations are Fourier-based methods. The only difference lies in their spectral remapping. Assuming horizontal plane waves only (i.e., no steering angle), one has the ERM speed $\hat{c} = c/\sqrt{2}$ [see (4)]. Now choosing $k_z =$

$2f/c$, i.e., $\hat{k}_z = \sqrt{2}f/c$, the spectral remapping for the f - k migration is yielded by (14):

$$f \rightarrow f_{f-k} = \text{sign}(f) \frac{c}{\sqrt{2}} \sqrt{k_x^2 + 2f^2/c^2}. \quad (18)$$

Again, assuming no steering angle, Lu's remapping is written as (see [25, Eq. 43]):

$$f \rightarrow f_{Lu} = f + \frac{c^2 k_x^2}{4f}. \quad (19)$$

A concise description of the theoretical background leading to this spectral remapping is available in [27]. Using a Taylor series about $(k_x, f) = (0, f_0)$, where f_0 is the central frequency, it can be shown that the two remapped frequencies are equivalent up to the third order; see the online supplementary materials for more details (Fig. 10). Lu's method and f - k migration thus mainly differ for relatively large spatial wavenumbers k_x . Fig. 10 illustrates how Lu's method and f - k migration behave in the Fourier domain; see also Fig. 10-bis in the online supplementary materials. Accordingly, one can observe that their spectra diverge when $|k_x| \gg 0$. On the contrary, the differences between the DAS and Lu's spectra are less significant and more homogeneous (see rightmost panels in Fig. 10).

3) *Further Details Regarding Lu's Method and Stolt's f - k Migration*: Lu's process assumes the scatterers to behave as pure monopole sources: as the plane wave reaches a scatterer, it becomes a source that emits circular waves spreading out uniformly in all directions. In such conditions, the Green's function for the 2-D wave equation is reduced to a Hankel function. When working in the Fourier domain, this leads to an analytical expression linking the received wavefront to the monopole source image. In reality, the scatterers behave more realistically as reflectors than monopole sources. The simplest model relating the wavefield to the reflectivity is precisely the exploding reflector model (ERM) as used in the f - k migration [8].

The Stolt's f - k migration is based on the ERM and provides an exact solution to the migration problem for constant wave speed [8], [10]. In the ERM, exploding sources are located along the reflecting interfaces. These sources explode in concert and emit waves which propagate upward and are recorded by the receivers at the surface [30]. In comparison with Lu's migration technique, the Stolt migration operates with upward waves only. The ERM model generates normal-incidence reflections. In other words, Stolt's model is basically a reflector model, whereas Lu's approach is based on a purely scattering model. The ERM, however, works for a zero-offset section; i.e., this model is valid only if each single element of the transducer emits independently (as for a standard synthetic aperture, see Section I). To make the ERM suitable for plane wave imaging, we had to modify the dif-

fraction hyperbolas by using basic spatial transformations (see Section II-A). This numerical step inevitably corrupts the exactness of the Stolt solution. However, because the fitting is performed up to third order in the vicinity of the hyperbola apex and because most of the signal energy is concentrated around the apex of the diffraction hyperbola, the Stolt's f - k migration remains highly accurate in PWI, as confirmed by our *in vitro* findings.

B. Plane Wave Imaging Versus Dynamic Focusing

An ultrasound image usually contains about a hundred lines. In conventional ultrasound, each scanline is generated by a single- or multi-transmit focused scheme. The state-of-the-art focused technique is dynamic focusing, which focuses both on transmission and reception [44], [45]. In the Verasonics system, receipt focusing is performed by a digital DAS beamformer and the image is divided into several focal zones. Multi-focus imaging is thus a slow process. Indeed, a total of [number-of-scanlines \times number-of-foci] transmit–receive sequences are required to get a single image. In comparison, only a few steered plane wave insonifications (typically 7 to 11 in this study) provides an image of quality comparable to dynamic focusing (see Figs. 7–9). Of particular importance is the repetitive acoustic energy concentration that occurs with transmit focusing. High acoustic peak pressures are generated by transmit-focusing techniques. In PWI, the acoustic pressure is uniformly spread over the insonified medium. As

an example, PWI thus helps to preserve microbubbles and improves ultrasound contrast imaging [46]. To sum up, conventional focus imaging is a high-energy, slow modality, whereas PWI is a low-energy, fast process.

C. PWI Using f - k Migration: Limitations and Perspectives

Ultrasound PWI needs the wavefronts to be planar and tilted with the desired incident angle. To get high-quality images by PWI, one must ensure that a planar wavefield is synthesized properly. An unlimited number of coplanar elementary sources can produce a perfect slant plane wave. In practice though, the amount of elements in a linear-array transducer is limited to 64, 128, or 192. This technical limitation may cause adverse effects that may negatively affect the resulting images. First, the wave equation is not limited to a plane and out-of-plane scatterers may thus contribute to the RF signals. More importantly, a more disturbing effect may rise from the grating lobes which are induced by the regular spacing of the individual transducer elements. It is known that the grating lobes are of larger magnitude as the steering angle increases [47]. This may explain in part why the migration was less efficient beyond 10° . Whether an appropriate transmit apodization can significantly reduce this adverse effect remains to be investigated. Besides the technical aspects, the f - k migration model is also subject to restrictions. This algorithm is based on the 2-D wave equation and the Born approximation, assuming a constant speed of sound and

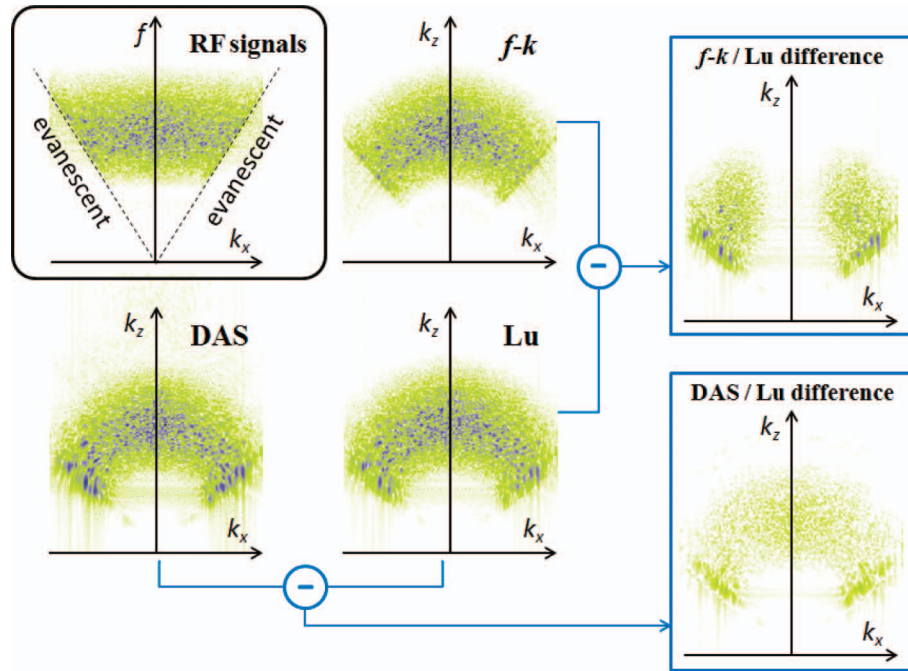


Fig. 10. Spectral mapping. Spectral mapping of the migrated images using the three techniques [delay-and-sum (DAS), Lu’s method, f - k migration]. The top left figure shows the spectrum of the raw RF signals before migration: k_x stands for the spatial wavenumber related to x and f is the temporal frequency. The empty region, where $|f/k_x| < c$, corresponds to the evanescent waves, which exhibit exponential decay in the very near-field. The rightmost figures represent the absolute differences of the Lu’s and f - k or DAS spectra. The RF signals were simulated using the freeware Field II [43] with randomly distributed scatterers. See also Fig. 10-bis in the supplementary materials.

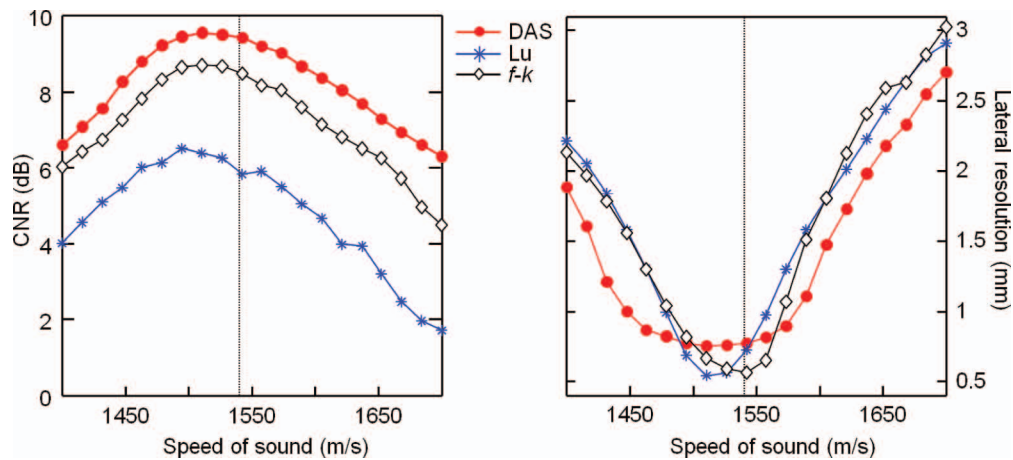


Fig. 11. Effect of speed-of-sound image on image quality. Contrast-to-noise ratio (CNR) of the 8-cm-deep cyst (left panel) and lateral resolution at 3 cm depth (right panel) for different values of speed of sound (*in vitro* results, see also Figs. 7 and 8). The vertical dashed line represents the speed of sound value given by the documentation of the Gammex phantom. 

only upcoming waves. In soft tissues, however, the speed of sound is not absolutely uniform [32] and one must therefore use an average or root-mean-square value. As with conventional focusing imaging [48], a mismatch in the speed of sound may significantly affect the quality of the images reconstructed by migration [49]. To illustrate the effect of a speed-of-sound mismatch in the context of plane wave imaging, image quality was determined in the Gammex phantom by repeating the migration processes with different speed values (the speed of sound within the Gammex phantom is claimed to be 1540 m/s). We studied the CNR of the 8-cm-deep cyst as well as the lateral resolution at 3-cm depth (see Sections III-C and III-D) for speeds of sound ranging from 1400 to 1700 m/s in the algorithms. B-mode images were generated using seven steering angles (-3° to $+3^\circ$). Our measures (Fig. 11) show that image quality indeed quickly degrades when the speed of sound is under- or over-estimated. CNR and lateral resolution, however, were little affected in the 1450 to 1550 m/s range.

Several correctors have been proposed to adjust the speed of sound in ultrasound imaging [50]–[52]. As a side note, because it is a constant-speed method, the Stolt’s f - k migration would be also limited in transcranial ultrasound imaging because the sound propagates much faster in the skull bone than in the brain. Less-limiting models valid for vertically varying velocities, such as the phase-shift method [19], [53], would be better adapted in this situation.

V. CONCLUSION

PWI offers the major advantage to yield high-quality images at very high frame rates with low acoustic energy. The Stolt’s f - k migration, which is based on a physically sound seismic technique, yields high-quality PWI-derived ultrasound images. An advantage of the f - k migration over the classical DAS is its faster computational speed, re-

sulting from the use of FFTs. More importantly, the f - k migration has the potential to return better lateral resolution. The Stolt’s f - k migration has thus the capability to significantly improve ultrasound PWI, and one could bet that PWI can look forward to a prosperous future in medical ultrasound. Further theoretical and experimental investigations will help to identify the best conditions for optimal PWI in different physiological contexts.

APPENDIX

A SIMPLIFIED MATLAB CODE FOR THE STOLT’S F - K MIGRATION WITH HORIZONTAL PLANE WAVES

A simplified Matlab code is provided for Stolt’s f - k migration of RF signals with PWI. Note that this program is simplified and works with horizontal plane waves only. In addition, the number of options is limited. A complete protected code with *in vitro* examples is provided in the supplementary materials or can be downloaded from D. Garcia’s webpage (www.biomecardio.com).

```
function migRF = ezfkmig(RF,fs,pitch)
```

```
%EZFKMIG f-k migration for plane wave imaging
% (Easy version)
%
% MIGRF = EZFKMIG(RFMAT,FS,PITCH) performs a f-k
% migration of the RF signals stored in the 2-D
% array RFMAT. MIGRF contains the migrated
% signals. FS and PITCH represent the sampling
% frequency (in Hz) and the pitch (in m) that
% were used to acquire the RF signals.
%
% The RF signals in RFMAT must have been
% acquired using a PLANE WAVE configuration with
% a linear array. Each column corresponds to a
% single RF signal over time acquired by a
% single transducer element.
```

```

%
% IMPORTANT NOTE:
% -----
% EZFKMIG is a simplified and non-optimized
% version of FKMIG. The code has been simplified
% for academic purposes. It only works with
% horizontal plane waves generated by a linear
% array, without delay in reception. The number
% of options with EZFKMIG is also limited. Use
% FKMIG for a more general application.
%
% Reference
% -----
% Garcia et al., Stolt's f-k migration for plane
% wave ultrasound imaging. IEEE UFFC, 2013
%
% See also FKMIG
%
% -- Damien Garcia -- 2013
% website: <a
% href="matlab:web(...
% 'http://www.biomecardio.com'...
% )">www.BiomeCardio.com</a>

```

```

[nt0,nx0] = size(RF);

% Zero-padding
nt = 2^(nextpow2(nt0)+1);
nx = 2*nx0;

% Exploding Reflector Model velocity
c = 1540; % propagation velocity (m/s)
ERMv = c/sqrt(2);

% FFT
fftRF = fftshift(fft2(RF,nt,nx));

% Linear interpolation
f = (-nt/2:nt/2-1)*fs/nt;
kx = (-nx/2:nx/2-1)/pitch/nx;
[kx,f] = meshgrid(kx,f);
fkz = ERMv*sign(f).*sqrt(kx.^2+f.^2/ERMv^2);
fftRF = interp2(kx,f,fftRF,kx,fkz,'linear',0);

% Jacobian (optional)
kz = (-nt/2:nt/2-1)/ERMv/fs/nt;
fftRF = bsxfun(@times,fftRF,kz)./(fkz+eps);

% IFFT & Migrated RF
migRF = ifft2(iftftshift(fftRF),'symmetric');
migRF = migRF(1:nt0,1:nx0);

```

BIBLIOGRAPHY

- [1] G. Montaldo, M. Tanter, J. Bercoff, N. Benech, and M. Fink, "Coherent plane-wave compounding for very high frame rate ultrasonography and transient elastography," *IEEE Trans. Ultrason. Ferroelectr. Freq. Control*, vol. 56, no. 3, pp. 489–506, Mar. 2009.
- [2] J. Bercoff, "Ultrafast ultrasound imaging," in *Ultrasound Imaging—Medical Applications*. New York, NY: InTech, 2011, pp. 3–24.
- [3] J. L. Gennisson, T. Deffieux, E. Mace, G. Montaldo, M. Fink, and M. Tanter, "Viscoelastic and anisotropic mechanical properties of in vivo muscle tissue assessed by supersonic shear imaging," *Ultrasound Med. Biol.*, vol. 36, no. 5, pp. 789–801, May 2010.
- [4] J. Bercoff, G. Montaldo, T. Loupas, D. Savery, F. Meziere, M. Fink, and M. Tanter, "Ultrafast compound Doppler imaging: Providing full blood flow characterization," *IEEE Trans. Ultrason. Ferroelectr. Freq. Control*, vol. 58, no. 1, pp. 134–147, Jan. 2011.
- [5] J. Udesen, F. Gran, K. Hansen, J. A. Jensen, C. Thomsen, and M. B. Nielsen, "High frame-rate blood vector velocity imaging using plane waves: Simulations and preliminary experiments," *IEEE Trans. Ultrason. Ferroelectr. Freq. Control*, vol. 55, no. 8, pp. 1729–1743, Aug. 2008.
- [6] J. Provost, V. T. Nguyen, D. Legrand, S. Okrasinski, A. Costet, A. Gambhir, H. Garan, and E. E. Konofagou, "Electromechanical wave imaging for arrhythmias," *Phys. Med. Biol.*, vol. 56, no. 22, pp. L1–L11, Nov. 2011.
- [7] E. Mace, G. Montaldo, I. Cohen, M. Baulac, M. Fink, and M. Tanter, "Functional ultrasound imaging of the brain," *Nat. Methods*, vol. 8, no. 8, pp. 662–664, Aug. 2011.
- [8] G. F. Margrave, "Elementary migration methods," in *Numerical Methods of Exploration Seismology*. CREWES Educational Resources, Ed. 2003, pp. 112–188. [Online]. Available: <http://www.crewes.org/ResearchLinks/FreeSoftware/NumMeth.pdf>
- [9] J. G. Hagedoorn, "A process of seismic reflection interpretation," *Geophys. Prospect.*, vol. 2, no. 2, pp. 85–127, 1954.
- [10] R. H. Stolt, "Migration by Fourier transform," *Geophysics*, vol. 63, no. 1, pp. 23–48, 1978.
- [11] G. F. Margrave, "Direct Fourier migration for vertical velocity variations," *Geophysics*, vol. 66, no. 5, pp. 1504–1514, 2001.
- [12] K. Nagai, "A new synthetic-aperture focusing method for ultrasonic B-scan imaging by the Fourier transform," *IEEE Trans. Sonics Ultrason.*, vol. 32, no. 4, pp. 531–536, Jul. 1985.
- [13] K. Mayer, R. Marklein, K. J. Langenberg, and T. Kreutter, "Three-dimensional imaging system based on Fourier transform synthetic aperture focusing technique," *Ultrasonics*, vol. 28, no. 4, pp. 241–255, Jul. 1990.
- [14] L. J. Busse, "Three-dimensional imaging using a frequency-domain synthetic aperture focusing technique," *IEEE Trans. Ultrason. Ferroelectr. Freq. Control*, vol. 39, no. 2, pp. 174–179, Mar. 1992.
- [15] Y. F. Chang and C. C. Chern, "Frequency-wavenumber migration of ultrasonic data," *J. Nondestruct. Eval.*, vol. 19, no. 1, pp. 1–10, 2000.
- [16] D. Vray, C. Haas, T. Rastello, M. Krueger, E. Brusseau, K. Schroeder, G. Gimenez, and H. Ermert, "Synthetic aperture-based beam compression for intravascular ultrasound imaging," *IEEE Trans. Ultrason. Ferroelectr. Freq. Control*, vol. 48, no. 1, pp. 189–201, Jan. 2001.
- [17] T. Stepsinski, "An implementation of synthetic aperture focusing technique in frequency domain," *IEEE Trans. Ultrason. Ferroelectr. Freq. Control*, vol. 54, no. 7, pp. 1399–1408, Jul. 2007.
- [18] A. J. Hunter, B. W. Drinkwater, and P. D. Wilcox, "The wavenumber algorithm for full-matrix imaging using an ultrasonic array," *IEEE Trans. Ultrason. Ferroelectr. Freq. Control*, vol. 55, no. 11, pp. 2450–2462, Nov. 2008.
- [19] M. H. Skjeltvareid, T. Olofsson, Y. Birkelund, and Y. Larsen, "Synthetic aperture focusing of ultrasonic data from multilayered media using an omega-k algorithm," *IEEE Trans. Ultrason. Ferroelectr. Freq. Control*, vol. 58, no. 5, pp. 1037–1048, May 2011.
- [20] C. Cafforio, C. Prati, and F. Rocca, "SAR data focusing using seismic migration techniques," *IEEE Trans. Aerosp. Electron. Syst.*, vol. 27, no. 2, pp. 194–207, 1991.
- [21] A. S. Milman, "SAR imaging by w - k migration," *Int. J. Remote Sens.*, vol. 14, no. 10, pp. 1965–1979, 1993.
- [22] M. Soumekh, "Reconnaissance with ultra wideband UHF synthetic aperture radar," *IEEE Signal Process. Mag.*, vol. 12, no. 4, pp. 21–40, 1995.
- [23] J. Y. Lu, "2D and 3D high frame rate imaging with limited diffraction beams," *IEEE Trans. Ultrason. Ferroelectr. Freq. Control*, vol. 44, no. 4, pp. 839–856, 1997.
- [24] J. Y. Lu, "Experimental study of high frame rate imaging with limited diffraction beams," *IEEE Trans. Ultrason. Ferroelectr. Freq. Control*, vol. 45, no. 1, pp. 84–97, 1998.

- [25] J. Cheng and J. Y. Lu, "Extended high-frame rate imaging method with limited-diffraction beams," *IEEE Trans. Ultrason. Ferroelectr. Freq. Control*, vol. 53, no. 5, pp. 880–899, May 2006.
- [26] P. Kruizinga, F. Mastik, N. de Jong, A. F. W. van der Steen, and G. van Soest, "Plane-wave ultrasound beamforming using a non-uniform fast Fourier transform," *IEEE Trans. Ultrason. Ferroelectr. Freq. Control*, vol. 59, no. 12, pp. 2684–2691, 2012.
- [27] D. L. D. Liu, "Plane wave scanning reception and receiver," U.S. Patent 6685641, Feb. 3, 2004.
- [28] D. Garcia. (2013, Aug.) BioméCardio website. [Online]. Available: <http://www.biomecardio.com/>
- [29] J. Gazdag and P. Sguazzero, "Migration of seismic data," *Proc. IEEE*, vol. 72, no. 10, pp. 1302–1315, 1984.
- [30] Ö. Yilmaz, "Migration," in *Seismic Data Analysis: Processing, Inversion, and Interpretation of Seismic Data*, vol. 1, Tulsa, OK: SEG Books, 2001.
- [31] A. Schuck and G. Lange, "Seismic methods," in *Environmental Geology*. Berlin, Germany: Springer, 2007, pp. 337–402.
- [32] M. O. Culjat, D. Goldenberg, P. Tewari, and R. S. Singh, "A review of tissue substitutes for ultrasound imaging," *Ultrasound Med. Biol.*, vol. 36, no. 6, pp. 861–873, Jun. 2010.
- [33] P. J. Beatty, D. G. Nishimura, and J. M. Pauly, "Rapid gridding reconstruction with a minimal oversampling ratio," *IEEE Trans. Med. Imaging*, vol. 24, no. 6, pp. 799–808, Jun. 2005.
- [34] W. Harlan, "Avoiding interpolation artifacts in Stolt migration," *Stanford Exploration Project*, vol. 30, pp. 103–110, 1982.
- [35] L. Greengard and J. Y. Lee, "Accelerating the nonuniform fast Fourier transform," *SIAM Rev.*, vol. 46, no. 3, pp. 443–454, 2004.
- [36] J. Song, Q. H. Liu, P. Torrione, and L. Collins, "Two-dimensional and three-dimensional NUFFT migration method for landmine detection using ground-penetrating radar," *IEEE Trans. Geosci. Rem. Sens.*, vol. 44, no. 6, pp. 1462–1469, 2006.
- [37] M. C. van Wijk and J. M. Thijssen, "Performance testing of medical ultrasound equipment: Fundamental vs. harmonic mode," *Ultrasonics*, vol. 40, no. 1–8, pp. 585–591, May 2002.
- [38] B. Y. S. Yiu, I. K. H. Tsang, and A. C. H. Yu, "GPU-based beamformer: Fast realization of plane wave compounding and synthetic aperture imaging," *IEEE Trans. Ultrason. Ferroelectr. Freq. Control*, vol. 58, no. 8, pp. 1698–1705, 2011.
- [39] H. Hassanieh, P. Indyk, D. Katabi, and E. Price, "Nearly optimal sparse Fourier transform," in *Proc. 44th Symp. Theory of Computing*, 2012, pp. 563–578.
- [40] D. Schneider, "A faster fast Fourier transform," *IEEE Spectr.*, vol. 49, no. 3, pp. 12–13, 2012.
- [41] W. A. Schneider, "Integral formulation for migration in two and three dimensions," *Geophysics*, vol. 43, no. 1, pp. 49–76, 1978.
- [42] D. L. Liu and R. C. Waag, "Propagation and backpropagation for ultrasonic wavefront design," *IEEE Trans. Ultrason. Ferroelectr. Freq. Control*, vol. 44, no. 1, pp. 1–13, 1997.
- [43] J. A. Jensen, "Field: A program for simulating ultrasound systems," *Med. Biol. Eng. Comput.*, vol. 34, suppl. 1, pt. 1, pp. 351–353, 1996.
- [44] G. Manes, P. Tortoli, F. Andreuccetti, G. Avitabile, and C. Atzeni, "Synchronous dynamic focusing for ultrasound imaging," *IEEE Trans. Ultrason. Ferroelectr. Freq. Control*, vol. 35, no. 1, pp. 14–21, 1988.
- [45] N. Wagner, Y. C. Eldar, A. Feuer, G. Danin, and Z. Friedman, "Xampling in ultrasound imaging," in *Proc. SPIE Medical Imaging*, 2011, vol. 7968, art. no. 796818.
- [46] O. Couture, M. Fink, and M. Tanter, "Ultrasound contrast plane wave imaging," *IEEE Trans. Ultrason. Ferroelectr. Freq. Control*, vol. 59, no. 12, pp. 2676–2683, 2012.
- [47] K. K. Shung and M. Zippuro, "Ultrasonic transducers and arrays," *IEEE Eng. Med. Biol. Mag.*, vol. 15, no. 6, pp. 20–30, 1996.
- [48] Q. Chen and J. A. Zagzebski, "Simulation study of effects of speed of sound and attenuation on ultrasound lateral resolution," *Ultrasound Med. Biol.*, vol. 30, no. 10, pp. 1297–1306, Oct. 2004.
- [49] S. H. Gray, J. Etegen, J. Dellinger, and D. Whitmore, "Seismic migration problems and solutions," *Geophysics*, vol. 66, no. 5, pp. 1622–1640, Sep. 2001.
- [50] M. E. Anderson and G. E. Trahey, "The direct estimation of sound speed using pulse-echo ultrasound," *J. Acoust. Soc. Am.*, vol. 104, no. 5, pp. 3099–3106, Nov. 1998.
- [51] F. R. Pereira, J. C. Machado, and W. C. A. Pereira, "Ultrasonic wave speed measurement using the time-delay profile of RF-back-scattered signals: Simulation and experimental results," *J. Acoust. Soc. Am.*, vol. 111, no. 3, pp. 1445–1453, Mar. 2002.

- [52] J. F. Krucker, J. B. Fowlkes, and P. L. Carson, "Sound speed estimation using automatic ultrasound image registration," *IEEE Trans. Ultrason. Ferroelectr. Freq. Control*, vol. 51, no. 9, pp. 1095–1106, Sep. 2004.
- [53] J. Gazdag, "Wave equation migration with the phase-shift method," *Geophysics*, vol. 43, no. 7, pp. 1342–1351, 1978.



Damien Garcia was born in 1974 in Paris, France. He obtained the D.E.A. and engineer degree from École Centrale de Marseille in 1997, and the M.Sc. and Ph.D. degrees in biomedical engineering from the University of Montreal in 2003. He was a postdoctoral fellow from 2006 to 2008 in the Department of Echocardiography, Gregorio Marañón hospital, Madrid, Spain. Dr. Garcia is director of the Research Unit of Biomechanics & Imaging in Cardiology (RUBIC) at the University of Montreal Hospital Research Centre (CRCHUM), and assistant professor at the Department of Radiology, Radio-Oncology and Nuclear Medicine at the University of Montreal. His research interests are in cardiovascular ultrasound imaging, Doppler echocardiography, image processing, mathematical and biomechanical modeling, fluid dynamics, and flow imaging. Damien Garcia holds a research scholarship from the Fonds de Recherche en Santé du Québec (FRSQ). A detailed list of his publications is available at www.biomecardio.com.



Louis Le Tarnec was born in 1986 in Boulogne Sur Mer, France. He joined the engineering school École Centrale de Paris in 2006 and then obtained a master's degree in applied mathematics. He worked for one year in the Research Unit of Biomechanics & Imaging in Cardiology (RUBIC) on image processing algorithms for ultrasound imaging. He is currently working in Paris, France, on numerical simulations for fluid mechanics applied to industrial issues such as transport of liquid methane or storage of radioactive waste.



Stéphan Muth received a bachelor's degree in image processing from the Institut Universtaire de Technologie de Caen, France, in 2006, and a master's degree in biomedical engineering from the Institut Supérieur d'Ingénieur de Franche Comté, France, in 2009. He joined the Research Unit of Biomechanics and Imaging in Cardiology (RUBIC), Montreal, in 2009 as a research assistant and worked on Doppler ultrasound, blood flow characterization, and plane wave imaging. He is currently orthopedic product manager in Biotech-Ortho, France.



Emmanuel Montagnon was born in 1982 in Nancy, France. He obtained his B.Sc. degree in theoretical physics from the University of Nantes, and his master's degree from the University of Grenoble in 2007. He is currently completing his Ph.D. studies in biomedical engineering at the University of Montreal, where he is conducting his research in the Laboratory of Biorheology and Medical Ultrasonics of the University of Montreal Hospital Research Center. His current research interests include dynamic ultrasound elastography and applications to breast cancer and deep vein thrombosis, shear wave scattering modeling, and plane wave imaging.

and applications to breast cancer and deep vein thrombosis, shear wave scattering modeling, and plane wave imaging.



Jonathan Porée received his B.Sc. degree in electrical engineering from the National Institute for Applied Sciences (INSA) in Rennes, France, in 2009. He then received, in 2010, his master's degree in imaging sciences from the National Institute for Applied Sciences (INSA) in Lyon. He is currently pursuing his Ph.D. degree in Biomedical Engineering at the University of Montreal. His current research, performed at the Laboratory of Biorheology and Medical Ultrasonics of the University of Montreal Hospital Research Center, includes developments in signal processing, motion analysis, and segmentation applied to ultrasound imaging.



Guy Cloutier (S'89–M'90–SM'07) obtained his B.Eng. degree in electrical engineering from the Université du Québec à Trois-Rivières in 1984, and M.Sc. and Ph.D. degrees in biomedical engineering from the École Polytechnique of Montreal, in 1986 and 1990, respectively. Between 1990 and 1992, he was a postdoctoral fellow at The Pennsylvania State University with Prof. K. Kirk Shung. Dr. Cloutier is Director of the Laboratory of Biorheology and Medical Ultrasonics at the University of Montreal Hospital Research Center (www.lbum-crchum.com), Professor and Director of research at the Department of Radiology, Radio-Oncology, and Nuclear Medicine at the University of Montreal. He is also a Member of the Institute of Biomedical Engineering at the University of Montreal. His research interests are in quantitative ultrasound imaging of red blood cell aggregation; quasi-static and dynamic ultrasound elastography of atherosclerotic plaques, vascular aneurysms, deep vein thrombi, and breast cancers; 3-D morphologic and hemodynamic assessment of lower-limb arterial stenosis; and mathematical and biomechanical modeling. He has published more than 140 peer-reviewed articles in these fields, holds 12 patents, and was recipient of the National Scientist award of the Fonds de la Recherche en Santé du Québec (2004–2009).

Supplementary materials for:

Stolt's f-k migration for plane wave ultrasound imaging

Damien Garcia^{1,2,3}, Louis Le Tarneac^{1,2}, Stéphan Muth^{1,2},
Emmanuel Montagnon^{2,4}, Jonathan Porée^{2,4} and Guy Cloutier^{2,3,4}

¹ RUBIC, Research Unit of Biomechanics and Imaging in Cardiology

² CRCHUM, Research Center, University of Montreal Hospital, Canada

³ Department of Radiology, Radio-Oncology and Nuclear Medicine,
and Institute of Biomedical Engineering, University of Montreal, Canada

⁴ LBUM, Laboratory of Biorheology and Medical Ultrasonics

email: Damien.Garcia@crchum.qc.ca, Garcia.Damien@gmail.com

website: www.biomecardio.com

Effect of the steering angle on the contrast

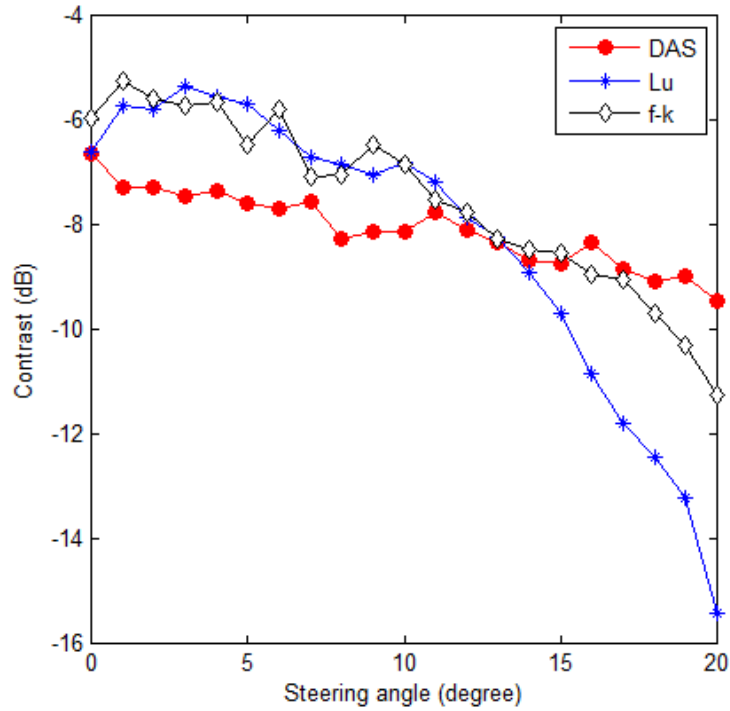


Figure 6.bis – Effect of the steering angle on the contrast. *In vitro* results. Contrast for a 6 mm-diameter 3 cm-deep anechoic target (using a Gammex phantom and the Verasonics scanner). The contrast remained almost unchanged up to 10° then decreased with angles > 10°. DAS: delay-and-sum; Lu: Lu’s method; *f-k*: *f-k* migration. See also Fig. 6 in the paper.

The contrast (in dB) was defined as:

$$C = 20 \log_{10} \frac{|\mu_t - \mu_b|}{(\mu_t - \mu_b)/2}$$

Effect of the number of compounding angles on the contrast

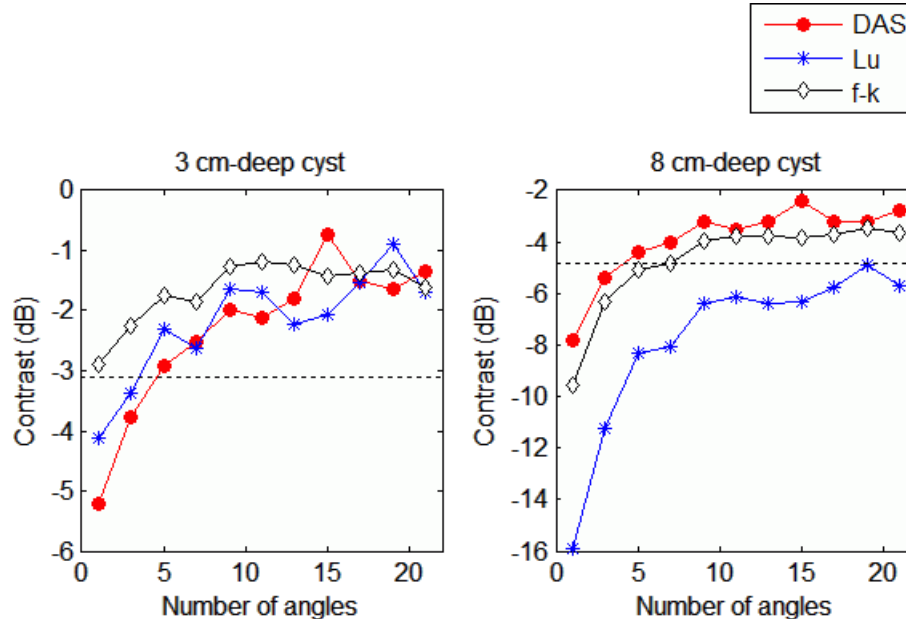


Figure 7.bis – Effect of the number of compounding angles on the contrast. *In vitro* results. Contrast for 6 mm-diameter 3 and 8 cm-deep anechoic targets (using a Gammex phantom and the Verasonics scanner). The targets of interest are delimited by dashed circles in Fig. 6 in the paper. Multi-angle compounding PWI provided contrast similar to those given by the dynamic focusing mode of the Verasonics scanner (black dashed horizontal lines). DAS: delay-and-sum; Lu: Lu’s method; *f-k*: *f-k* migration. See also Fig. 7 of the paper.

The contrast (in dB) was defined as:

$$C = 20 \log_{10} \frac{|\mu_t - \mu_b|}{(\mu_t - \mu_b)/2}$$

Lu's method vs. f - k migration: spectral mapping

We seek the (k_x, k_z) maps of the migrated RFs. Assuming horizontal plane waves only, we have $\hat{c} = c/\sqrt{2}$ (see Eq. 7 and 9). We define the wavenumber $k = f/c$. We neglect the evanescent waves, so that $|k| \geq |k_x|$. Note also that $\hat{k}_z/\hat{c} = k_z/c$.

1) Remapping

Both Lu and f - k migrations are spectral methods based on the 2-D wave equation. The only difference lies in the spectral remapping. Assuming horizontal plane waves only and choosing $k_z = 2k$, the remapping for the f - k migration is yielded by equation (14):

$$f \rightarrow f_{f-k} = \text{sign}(f) \frac{c}{\sqrt{2}} \sqrt{k_x^2 + 2f^2/c^2}. \quad (18)$$

For Lu's method, one has (see Eq. 43 in Cheng and Lu, *IEEE UFFC*, vol. 53, 2006):

$$f \rightarrow f_{Lu} = f + \frac{c^2 k_x^2}{4f}. \quad (19)$$

A Taylor series about $(k_x, f) = (0, f_0)$, where f_0 is the central frequency, yields:

$$f_{f-k} = f + \frac{c^2(f-2f_0)(f^2-2ff_0+2f_0^2)k_x^2}{4f_0^2} + O(k_x^4(f-f_0)^4), \quad (20)$$

and

$$f_{Lu} = f + \frac{c^2(f-2f_0)(f^2-2ff_0+2f_0^2)k_x^2}{4f_0^2} + O(k_x^4(f-f_0)^4). \quad (21)$$

The two remapped frequencies are thus equivalent up to the third order about $(k_x, f) = (0, f_0)$. This is visible on Fig. 10 (rightmost top panel).

2) Spectral mapping of the migrated RFs

2.a) Stolt's f - k migration

The wavenumber \hat{k}_z , associated to the ERM model is given by Eq. (12). Because $\hat{k}_z/\hat{c} = k_z/c$, Eq. (12) becomes:

$$k_z^2 = k^2 - k_x^2/2. \quad (22)$$

Equation (22) gives the relationship between the (k_x, k) and (k_x, k_z) maps, which are the spectral maps before and after migration, for the Stolt's f - k migration.

2.b) Lu's method

The k_z 's can be deduced from Eq. 43 in [Cheng and Lu, *IEEE UFFC*, vol. 53, 2006]. Considering horizontal plane waves only, one gets:

$$k_z = \left(k + \sqrt{k^2 - k_x^2} \right) / 2 . \quad (23)$$

Equation (23) gives the relationship between the (k_x, k) and (k_x, k_z) for the Lu's method. One can now compare the spectral maps yielded by the two migration methods (see Fig. 10.bis).

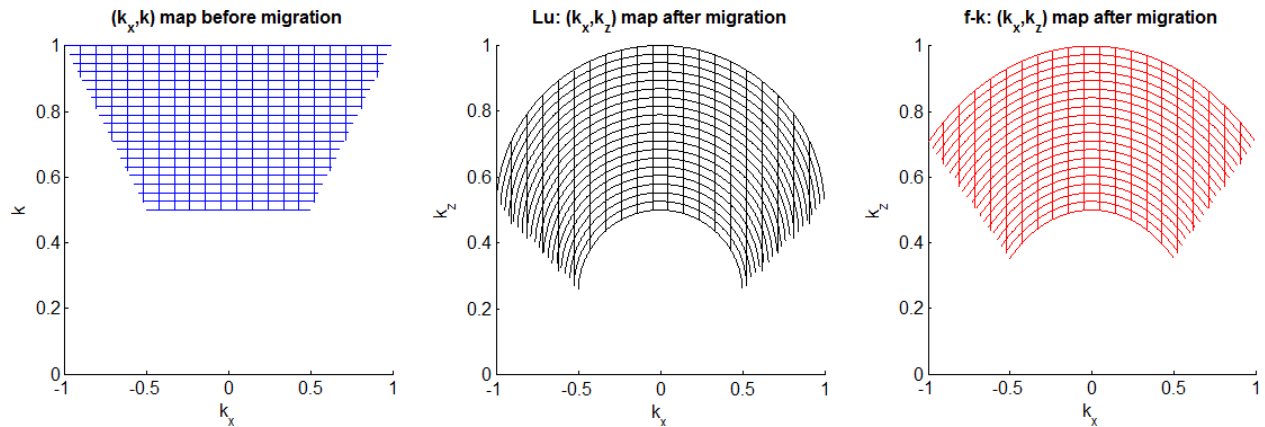


Figure 10.bis – Spectral mapping. Spectral mapping of the Lu- and f - k migrated images (arbitrary units). The left figure shows the spectrum of the raw RF signals before migration around the central frequency. The empty region, where $|k/k_x| < 1$, corresponds to the evanescent waves. The central and right figures represent the Lu's and f - k spectra, respectively. See also Fig. 10 of the paper.